Target identification in terrestrial laser scanning

X. Ge* and T. Wunderlich

Target identification is an important process in terrestrial laser scanner (TLS) measurements; however, due to strong competition between manufacturers, the design of laser scanners is kept secret and is usually strengthened by accompanying proprietary software. Moreover, the target identification algorithms (i.e. definitions of the target centre) are not specified. This makes it difficult for users to objectively compare scanners from different manufacturers and to judge the reliability of the captured scan data by a brand scanner and accompanying software. This paper presents a unified general method to complete the process of target identification. The proposed method consists of four major steps: first, determination of the target plane; second, classification of the reflection intensity values and extraction of the border between white and black; third, detection and elimination of erroneous points from step two; and fourth, fitting of the intersection lines and calculation of the centre of the two lines. Because TLS is a reflectorless surveying model that can receive hundreds of signals, its measurements require more stringent objective conditions than traditional measurement by total stations (TS). Therefore, robust estimation methods are used to reduce the influence of random errors; moreover, the model of error-in-value (EIV) is also introduced to deal with captured data. Finally, the target's centre can be obtained from an iteration process. For the experiments, a Leica HDS 7000 terrestrial laser scanner, with its accompanying software, Cyclone, and a Leica Laser Tracker AT901were employed. The performance of the proposed method is compared with Cyclone and some early methods from published studies at different resolutions and distances. The paper concludes that the proposed method can obtain reliable results at the same level of accuracy level as those obtained using accompanying software; thus, it provides an objective means to compare the quality of different scanners. The advantage is that our method only makes use of information provided by all scanners and does not require additional proprietary information that cannot be accessed.

Keywords: Terrestrial laser scanner, Target identification, Surveying engineering, Reflected intensity

Introduction

Terrestrial laser scanning (TLS) is a technique that remotely obtains the spatial coordinates of an object using laser light and has become a standard surveying procedure in the architecture, engineering, and construction sectors with a wide range of applications (Gordon and Lichti, 2007; Tristan, 2011; Ebeling *et al.*, 2011). However, the application of TLS has some limitations. On the one hand, information from TLS is always expressed by a vast point cloud of 3D coordinates with a relatively random distribution on the object's surface, preventing a one-to-one correspondence from spots to points. Thus, captured scan data cannot be directly exploited in engineering projects to extract coordinates of a specific object point. On the other hand, TLS measurements require more stringent objective conditions. Researchers have classified the errors in TLS into mainly two categories: internal and external (Lichti and Gordon, 2004; Gordon, 2005; Staiger, 2005) with the latter, i.e. temperature, atmospheric scintillation, dust, distance, reflectance, and spot size, largely affecting the accuracy of the point cloud, which is supported by Granthamn *et al.* (1997), Lichti and Harvey (2002) and Thiel and Wehr (2004). Therefore, to enable accurate registration and georeferencing of point clouds, special targets are usually employed to provide virtual centre coordinates through automatic extraction algorithms. Any uncertainty in these centre coordinates will directly affect the accuracy of the entire project. According to the above, the accuracy of the TLS surveys is to a great extent limited by the target identification quality.

Faculty of Civil Engineering and Surveying, Technical University of Munich. Arcisstraße 21, 80333 Munich, Germany

*Corresponding author, email xuming.ge@tum.de

Received 15 September 2013; accepted 5 March 2014
DOI 10.1179/1752270614Y.0000000097

Owing to patent protection and strong competition, we cannot access the core of the instrumental system information and the proprietary software algorithms. Without an objective public approach, it is difficult for users to select an appropriate terrestrial laser scanner for their engineering projects in the fast-paced laser scanner market, which has a great variety of measurement systems and a near annual updating of well known and improved models showing more and more promising specifications. Moreover, different reference standards also provide further difficulties in the investigation of instrument calibration. Although not very well documented, the topic of target identification has been addressed previously in published literature (Lichti *et al.*, 2000; Gordon *et al.*, 2001; Valanis and Tsakiri, 2004; Kersten *et al.*, 2004). Lichti *et al.* (2000) proposed three radiometric approaches based on intensity to define the target centre as the position with the maximum radiance, the radiometric centre of the four strongest returns, and the radiometric centre of all returns. In later references, the third method has been proved to perform better than the other two; however, it cannot render reliably accurate results. In Valanis *et al.* (2004) the C-Means method was used to extract the target centre, and the results described are better than those obtained by previous methods. In all the published literature, the results by scanner accompanying software are considered as the true or best centre values, and can then be used to verify the proposed methods. Although the results by accompanying software currently seem to be the best choice and assumed to be the virtual 'true' value of the target, the different resolutions may also force the accompanying software to produce errors. To the authors' knowledge, there are no documents discussing accompanying software performance over different resolutions or comparisons with self-proposed methods. The purpose of the paper is to propose a new method for laser scanner target identification and to compare its performance over different resolutions and distances with that of the accompanying software. Although there are also other geometric shapes of targets (e.g. spheres, cylinders), we restrict ourselves here to quadrants plane targets. Here we should point out that the quadrants plane targets are mainstream targets currently in the TLS market which are more accurate than the older circle targets. Furthermore, the plane targets are easy to use and more economical than the sphere and cylinder targets especially when you need a lot of targets in your project (e.g. self-calibration see Reshetyuk, 2006, 2010; Lichti, 2007).

The rest of the paper is organised as follows. In the section on 'Target plane fitting', we will introduce the iterative formulae of weighted total least squares to solve target fitting. The design of the weighted matrix for all observations will be described in detail. Furthermore, the reflection and refraction errors that may be caused by material properties of the object, surface colour, moisture of the surface, and so on, and the planarity condition of the resulting plane will be considered, and a robust estimation will be discussed. Section on 'Threshold of intensity and centre identification' will describe a concept for appropriate reflected intensity values for the captured scan data and will present an iterative calculation method to obtain a reliable target centre. Section on 'Influence of incidence angle' will discuss the influence of incidence angle in the target identification. The real experiments are carried out in the section on 'Application examples' to demonstrate the performance and efficiency of the developed method. Finally, remarks will conclude the paper in the section on 'Conclusions'.

Target plane fitting

The plane model is defined by

$$\mathbf{z} = a\mathbf{x} + 1b\mathbf{y} + c \tag{1}$$

Rewritten as an observation equation

$$\mathbf{z} + \mathbf{v}_z = [\mathbf{x} \quad \mathbf{y} \quad 1] \begin{bmatrix} a \\ b \\ c \end{bmatrix} = \mathbf{A}\boldsymbol{\beta} \tag{2}$$

where $\mathbf{z}=n\times 1$ is a vector of observed $\mathbf{z}$ coordinates, $\mathbf{v}_z=n\times 1$ is a residual vector of the observations, $\mathbf{A}=n\times 3$ is the design matrix, and $\boldsymbol{\beta}=3\times 1$ is a vector of unknown parameters. Clearly, $\mathbf{x}$, $\mathbf{y}$ in the design matrix are the same coordinate components as in the observation vector $\mathbf{z}$, so it is improper to neglect their errors in the calculation. Rewriting the observation equation

$$\mathbf{z} + \mathbf{v}_z = ([\mathbf{x} \quad \mathbf{y} \quad 1] + \mathbf{E}_A) \begin{bmatrix} a \\ b \\ c \end{bmatrix} \tag{3}$$

where $\mathbf{E}_A=n\times 3$ represents the residual matrix of the design matrix $\mathbf{A}$. Then, the restriction turns to the weighted total least squares

$$\min\left(\mathbf{v}_z^T\mathbf{P}_z\mathbf{v}_z + \mathbf{e}_A^T\mathbf{P}_A\mathbf{e}_A\right) \tag{4}$$

where $\mathbf{P}_z=n\times n$ means the weight matrix of the observation vector, $\mathbf{P}_A=3n\times 3n$ represents the weighted matrix of the design matrix, and $\mathbf{P}_A=\mathbf{P}_0:\mathbf{P}_X$ where : expresses the Kronecker product. $\mathbf{P}_0$ and $\mathbf{P}_X$ represent the column vector's weighted matrix and the row vector's weighted matrix of the design matrix respectively. $\mathbf{e}_A=vec(\mathbf{E}_A)$ and $vec(\bullet)$ are to reconstruct a matrix as a vector (Konstantinov *et al.*, 2000). In the captured scan data, we assume each returned point to be independent of the others and the coordinate errors to have zero mean, but the coordinate components of a point to be correlated. Then, writing the observation vector's cofactor matrix as

$$\mathbf{Q}_Z = \begin{bmatrix} \sigma_{z_1}^2 & & & \\ & \sigma_{z_2}^2 & & \\ & & \ddots & \\ & & & \sigma_{z_n}^2 \end{bmatrix} \tag{5}$$

where $\sigma_{z_1}^2$ is the variance of the z-coordinate component of the first point. The column vector's and row vector's cofactors of the design matrix are respectively

$$\mathbf{Q}_0 = \begin{bmatrix} \sigma_x^2 & \sigma_{xy}^2 & \\ \sigma_{xy}^2 & \sigma_y^2 & \\ & & \kappa \end{bmatrix} \tag{6}$$

$$\mathbf{Q}_X = \begin{bmatrix} H_1 & & & \\ & H_2 & & \\ & & \ddots & \\ & & & H_n \end{bmatrix}_{n\times n} \tag{7}$$

where σ_x^2 and σ_y^2 represent the mean value of the variances of the x- and y-axis coordinate components respectively, and σ_{xy}^2 is the mean value of the co-variance. κ is an epsilon like $\kappa=10^{-12}$ that means the third column of the design matrix is error free. In equation (7) $H_i=\sigma_{x_i}^2+\sigma_{y_i}^2$ and $\sigma_{x_i},\sigma_{y_i}$ express the variances of the x-axis and y-axis coordinate components of the ith point respectively. As the points are independent, the off-diagonal elements in equations (5) and (7) are all assumed zeros. In equation (4) $\mathbf{v}_z^T\mathbf{P}_z\mathbf{v}_z\geq 0$ and $\mathbf{e}_A^T\mathbf{P}_A\mathbf{e}_A\geq 0$; thus, we can simply obtain the inequality as

$$\begin{aligned}&\min\left(\mathbf{v}_z^T\mathbf{P}_z\mathbf{v}_z+\mathbf{e}_A^T\mathbf{P}_A\mathbf{e}_A\right)\geq\\&\min\left(\mathbf{v}_z^T\mathbf{P}_z\mathbf{v}_z\right)+\min\left(\mathbf{e}_A^T\mathbf{P}_A\mathbf{e}_A\right)\end{aligned}\tag{8}$$

Assuming the equality holds, the problem in equation (4) translates to solving two independent minimum problems. The first element at the right hand-side of equation (8) is the classical least squares problem and the cofactor matrix for the observation vector as equation (5), and the second element at the right hand-side of equation (8) is the data for the least squares problem and the weighted matrix for the design matrix as $\mathbf{P}_A$. Therefore, in the above process, coordinate component z seems to be independent from coordinate components x and y, which means the values of covariance between x-z and y-z have little influence in the calculation of our model.

From the laser scanning measurement principle, we can obtain each coordinate component's variance–covariance

$$\begin{cases}x=r\cos\theta\cos\varphi\\y=r\cos\theta\sin\varphi\\z=r\sin\theta\end{cases}$$

$$\begin{bmatrix}\sigma_x^2&\sigma_{xy}^2&\sigma_{xz}^2\\\sigma_{xy}^2&\sigma_y^2&\sigma_{yz}^2\\\sigma_{zx}^2&\sigma_{zy}^2&\sigma_z^2\end{bmatrix}=\mathbf{JCJ}^T\tag{10a}$$

$$\mathbf{J}=\begin{bmatrix}\frac{\partial x}{\partial r}&\frac{\partial x}{\partial\theta}&\frac{\partial x}{\partial\varphi}\\\frac{\partial y}{\partial r}&\frac{\partial y}{\partial\theta}&\frac{\partial y}{\partial\varphi}\\\frac{\partial z}{\partial r}&\frac{\partial z}{\partial\theta}&\frac{\partial z}{\partial\varphi}\end{bmatrix}\quad\text{and}\tag{10b}$$

$$\mathbf{C}=\begin{bmatrix}\sigma_r^2&&\\&\sigma_\theta^2+\sigma_{beam}^2&\\&&\sigma_\varphi^2+\sigma_{beam}^2\end{bmatrix}$$

where r, θ, and φ are the range and vertical and horizontal angles of the TLS beam, respectively, and σ_r^2, σ_θ^2, and σ_φ^2 are the respective variances, which can be obtained, for example, from the manufacturer's specification. σ_{beam}^2 is the accuracy of laser divergence, is the uncertainty due to the beam width (Lichti and Gordon, 2004). The impact is not obvious over short distances but will show up over longer distances.

We introduced the iterative weighted total least squares by Schaffrin and Wieser (2008) to the calculation as follows:

1. Calculate $\hat{\boldsymbol{\beta}}^{(0)}$ using Least squares method, and $\hat{\boldsymbol{\upsilon}}^{(0)}=0$

$$\hat{\boldsymbol{\beta}}^{(1)}=\left\{\mathbf{A}^T\left[\mathbf{Q}_Z+\left(\hat{\boldsymbol{\beta}}^{(0)^T}\mathbf{Q}_0\hat{\boldsymbol{\beta}}^{(0)}\right)\mathbf{Q}_X\right]^{-1}\mathbf{A}\right\}^{-1}\mathbf{A}^T\left[\mathbf{Q}_Z+\left(\hat{\boldsymbol{\beta}}^{(0)^T}\mathbf{Q}_0\hat{\boldsymbol{\beta}}^{(0)}\right)\mathbf{Q}_X\right]^{-1}\mathbf{z}\tag{11}$$

2. Calculate new $\hat{\boldsymbol{\upsilon}}$ and new $\hat{\boldsymbol{\beta}}$ using the following equations

$$\boldsymbol{\lambda}^{(i)}=\left(\mathbf{Q}_Z+\left(\hat{\boldsymbol{\beta}}^{(i)^T}\mathbf{Q}_0\hat{\boldsymbol{\beta}}^{(i)}\right)\mathbf{Q}_X\right)^{-1}(\mathbf{z}-\mathbf{A})\hat{\boldsymbol{\beta}}^{(i)}\tag{12}$$

$$\hat{\boldsymbol{\upsilon}}^{(i)}=\boldsymbol{\lambda}^{(i)^T}\mathbf{Q}_X\boldsymbol{\lambda}^{(i)}\tag{13}$$

$$\hat{\boldsymbol{\beta}}^{(i+1)}=\left\{\mathbf{A}^T\left[\mathbf{Q}_Z+\left(\hat{\boldsymbol{\beta}}^{(i)^T}\mathbf{Q}_0\hat{\boldsymbol{\beta}}^{(i)}\right)\mathbf{Q}_X\right]^{-1}\mathbf{A}-\hat{\boldsymbol{\upsilon}}^{(i)}\mathbf{Q}_0\right\}^{-1}\mathbf{A}^T\left[\mathbf{Q}_Z+\left(\hat{\boldsymbol{\beta}}^{(i)^T}\mathbf{Q}_0\hat{\boldsymbol{\beta}}^{(i)}\right)\mathbf{Q}_X\right]^{-1}\mathbf{z}\tag{14}$$

where the superscript (i) denotes the iteration count

3. Repeat Step 2 until $\left\|\hat{\boldsymbol{\beta}}^{(i+1)}-\hat{\boldsymbol{\beta}}^{(i)}\right\|\leq\delta_0$, where δ_0 is the given threshold
4. Obtain the vectors of the unknown parameters after the iteration as follows

$$\hat{\boldsymbol{\beta}}_{WTLS}=\hat{\boldsymbol{\beta}}^{(i+1)}\tag{15}$$

In the aforementioned algorithm, $\boldsymbol{\lambda}$ is a Lagrange factor, $\hat{\boldsymbol{\upsilon}}$ is an intermediate variable, and δ_0 is the threshold; here we give $\delta_0=10^{-6}$. In the whole process, a threshold ε serves to control the planarity of the resulting plane; in other words, the point will be removed if the distance to the resulting plane exceeds the given threshold. The value of the threshold mainly depends on scanning resolution, distance, and material properties of the object. In the following experiments, we accept the threshold from 1 to 2 mm corresponding to different resolutions. The aforementioned iterative algorithm is repeated, and the threshold is applied to judge the robustness of the captured plane until the entire calculation progresses to convergence.

Threshold of intensity and centre identification

Reflected intensity is one common information parameter we can obtain from the captured scan data with a range of -2047 to $+2048$. To make the calculation easier and to avoid non-convergence, the intensity range is mapped linearly to the interval of 0 to 1 as follows

$$\bar{I}=\frac{(I\cdot 0\cdot 3037+621\cdot 8729)}{1244}\tag{16}$$

where I is the original intensity value and $\bar{I}$ is the processed value. Figure 1 shows the point cloud of a target with its property of reflected intensity from an x-z perspective. It is clear that the target is regularly divided

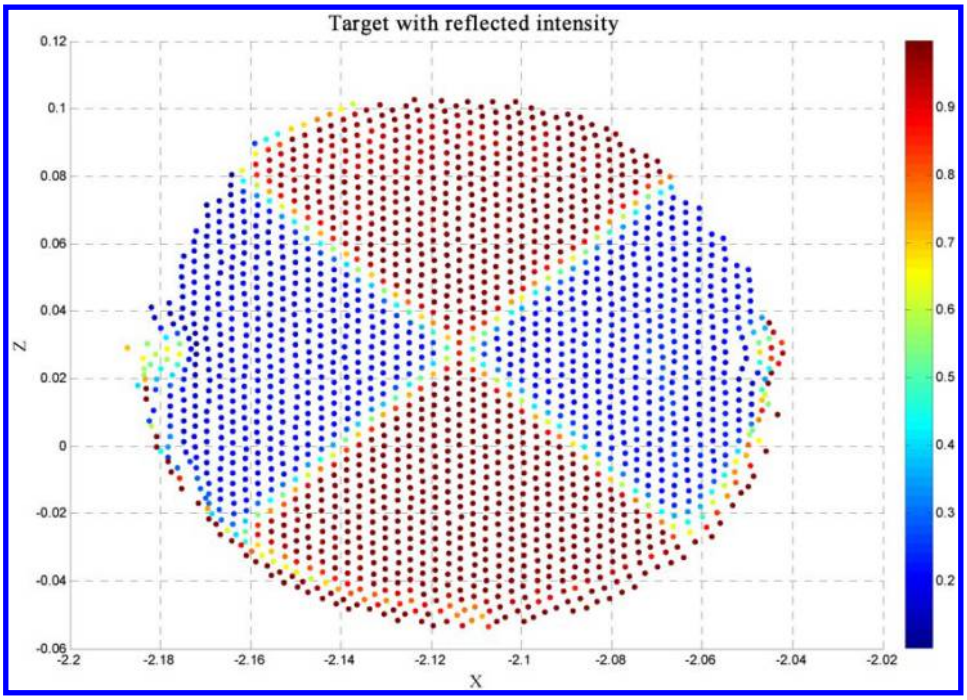

1 Target's point cloud with reflected intensity

into three categories by the reflected intensity, the first category corresponds to the white area of the target with values of intensity approximately over 0·9; the second category corresponds to the black area of the target with that value approximately below 0·3; the rest of the points with an intensity range between 0·3 and 0·9 are classified as the third category, which we called 'middle value (MV)' in this paper (see Fig. 2), and those points mainly appear at the junction of black and white areas and also at some parts near the edges. In the example, 0·3 and 0·9 are given as thresholds that show the lower and upper limits respectively, to select the appropriate point cloud in the later section. The lower and upper limit depend on the resolution and distance in each scanning measurement, but show only slight changes in different situations. Figure 3 shows the tests related to the distribution of reflected intensity of target with different resolution within a range of 20 m, using the Leica HDS 7000 laser scanner. Evidently, all intensity histograms have two peaks, except the last two figures in the first row with middle resolution and over 15 m. The upper limit rests stably at about 0·9, and the lower limit is approximately in the range of 0·3 to 0·4. Selecting the points with an MV of intensity in the point cloud to calculate the target centre, see the points with red circles in Fig. 4.

According to the discussion above, the points with an MV of intensity do not only appear at the border between black and white, they are also at some parts of the target's edges, see Fig. 4. As the target radius is known, we can easily reduce the impact of the edge noise in the centre calculation. Exploiting the mean value of the whole target point cloud as an approximate target centre, called the mean value centre (MVC), the distance of each point to MVC can be calculated, giving a

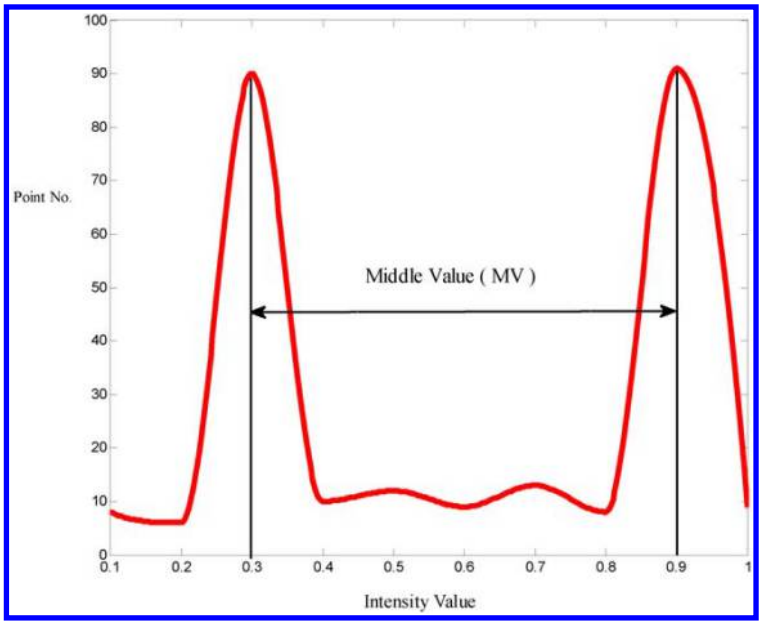

2 'MV' of intensity

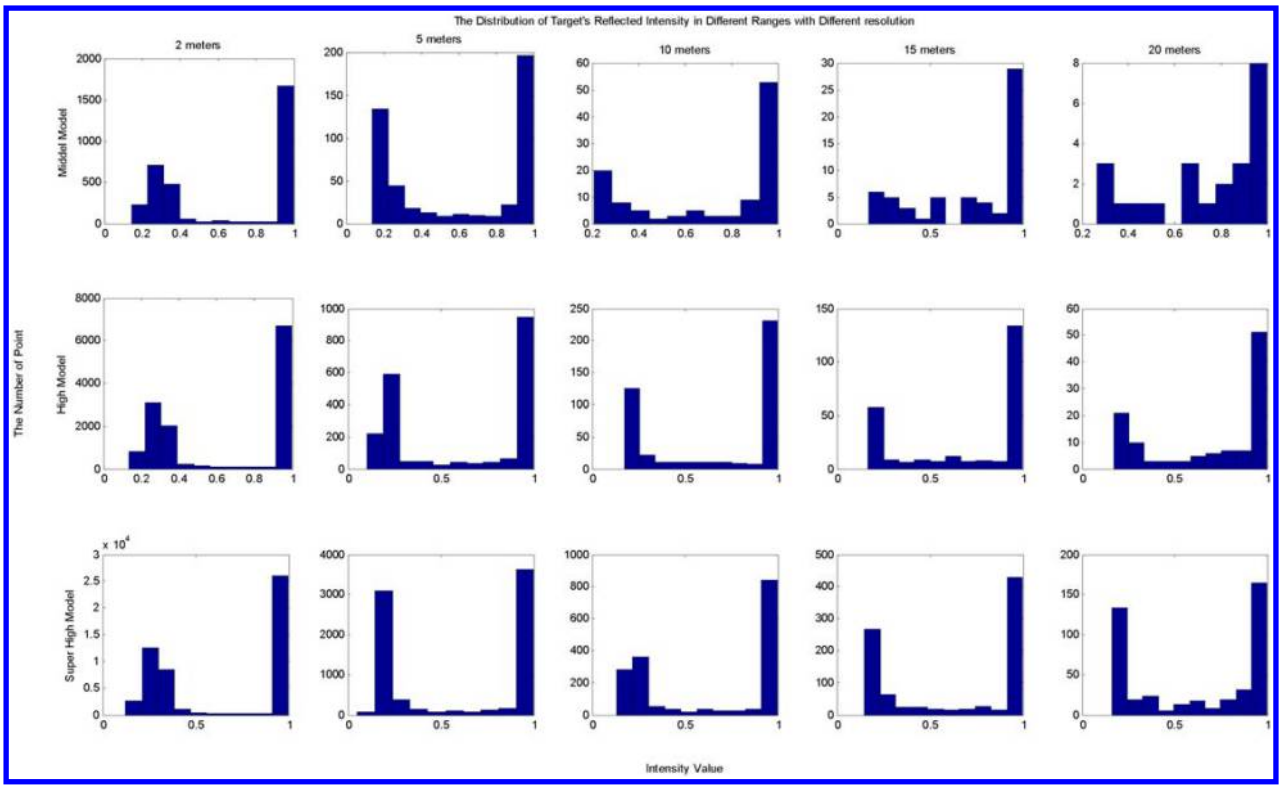

3 Property of intensity with different resolutions and distances

distance threshold smaller than the target's radius to produce a safe range, finally deleting the outside points. It does not prove necessary to complete this process with high accuracy because the loss of some non-edge points does not affect centre identification in our approach. Then, the remaining points are projected to the resulting plane so as to transform 3D coordinates to 2D plane coordinates. Figure 5 displays an example of the projection result. Obviously, after accurate fitting of two intersecting lines, the centre of the target can be obtained. However, setting intensity thresholds cannot always remove all improper points, in other words, there are some noise points with MV of intensity not belonging to the two lines, for example, when scanning at short distance with higher resolution. Figure 6 shows this with scans within 2 m at a super high resolution. Taking into account the above mentioned problem, the M estimate method is applied in the calculation. First, the MVC is used as the initial value of the target's centre, and then the entire area is divided into four

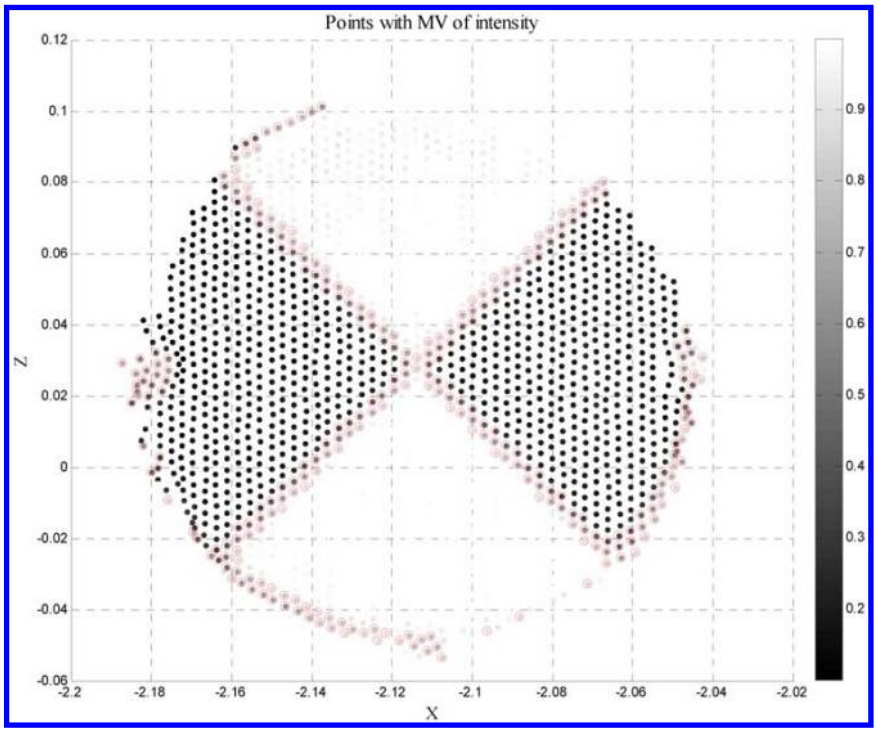

4 Selected points with 'MV' of intensity

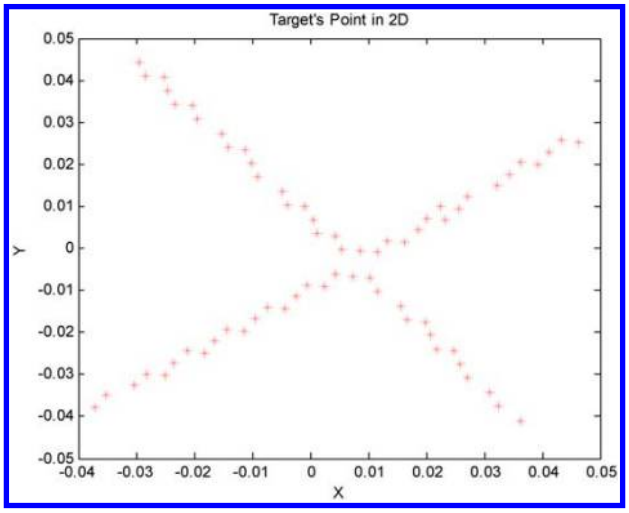

5 Point cloud in 2D system

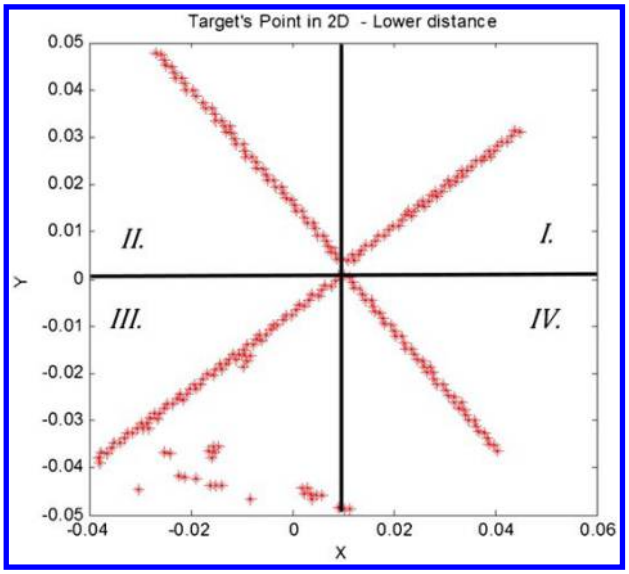

6 Point cloud in 2D system with some noise and its quadrants divided

quadrants, also see Fig. 6. Second, apply the data in the first and third quadrants to fit the first line and the data in the remaining quadrants to fit the second line respectively. Third, calculate the intersection to replace the centre in step 1 and repeat steps 1 to 3 until the entire process converges. The weighted total least squares technique is applied again to calculate these two lines, and the restriction is the same as in equation (4). The observation equation reads

$$\mathbf{y}+\mathbf{v}_{\mathrm{y}}=([1 \quad \mathbf{x}]+\mathbf{E}_{\mathrm{A}})\begin{bmatrix} d \\ e \end{bmatrix} \tag{17}$$

where $\mathbf{E}_{\mathrm{A}}=n\times 2$ is the residual matrix of the design matrix $\mathbf{A}$, and $\mathbf{v}_{\mathrm{y}}=n\times 1$ represents the residual vector of the observations. d and e are two unknown parameters. The weighted matrices of the design matrix and the observation vector are given as in equations (5)–(7), using variance of coordinate components. In order to solve the problem of some points with MV of intensity not belonging to the two lines, we apply the weigh kernel function (Zhou, 1989) to reweigh each point after each iteration

$$\omega_{\mathrm{i}}=\begin{cases} 1 & |r_{\mathrm{i}}|\le 1{\cdot}5\hat{\sigma}_0 \\ \dfrac{1{\cdot}5\hat{\sigma}_0}{|r_{\mathrm{i}}|} & 1{\cdot}5\hat{\sigma}_0<|r_{\mathrm{i}}|\le 2{\cdot}5\hat{\sigma}_0 \\ 0 & |r_{\mathrm{i}}|>2{\cdot}5\hat{\sigma}_0 \end{cases} \tag{18}$$

where r_{i} is the residual of linear fitting and $\hat{\sigma}_0$ is the posterior standard deviation of each iteration. Based on Schaffrin and Wieser (2008), the posterior standard deviation can be calculated by

$$\hat{\sigma}_0=\left(\frac{\mathbf{v}_{\mathrm{y}}^{\mathrm{T}}\mathbf{P}_{\mathrm{y}}\mathbf{v}_{\mathrm{y}}+\mathbf{e}_{\mathrm{A}}^{\mathrm{T}}\mathbf{P}_{\mathrm{A}}\mathbf{e}_{\mathrm{A}}}{n-2}\right)^{1/2} \tag{19}$$

where $\mathbf{P}_{\mathrm{y}}$ and $\mathbf{P}_{\mathrm{A}}$ are weight matrices of the observation vector and the design matrix respectively, in the process of linear fitting. $\mathbf{e}_{\mathrm{A}}$ has the same definition as before. The residual is the vertical distance from the point to the resulting line when applying the total least squares technique in linear fitting.

Influence of incidence angle

The precision of the target centre identification depends on the identification algorithm, but also largely on the quality of the point cloud. As we know, the quality of the point cloud is derived based on the individual point precision per scan and the individual point signal to noise ratio (SNR) is affected by the incidence angle. There are several previous TLS studies (Kremen *et al.*, 2006; Kaasalainen *et al*, 2005) which focus on the influence of the incidence angle in TLS. Soudarissanane *et al.* (2009, 2011) reported that the incidence angle had a cosine effect on the precision of laser points and modelled the incidence angle contribution to the total error budget of a TLS. The most important conclusion from previous studies is that the received signal level of the measurements decreases with increasing incidence angles and the received signal level influences the precision of the distance measurement. Figure 7 shows the Leica HDS7000 scanner's theoretical errors in distance measurements when the incidence angle increases from 0 to 90°. Two main points can be found from Fig. 7:

(i) when the incidence angle is larger than 60° the error becomes obvious
(ii) the error increases proportional to the distance measured.

In our proposed approach, the target centre identification is derived based on the reflected intensity of the individual point. The increasing incidence angle does not only influence the precision of the distance measurement but also the reflected intensity. Figure 8 gives the distribution of the target's reflected intensity when the incidence angle increases from 10 to 70°. The first row shows the results scanned by high resolution and the second row those by super high resolution. Compared with Fig. 3, it is obvious that the overall range of the reflected intensity is reduced and continues to decrease with increasing incidence angle. However, the most important conclusion from Fig. 8 is that there still exists a MV of intensity when the incidence angle increases and the range of reflected intensity continues to decrease. Thus, when the target is not pointed directly normal to the scanner, we can choose suitable thresholds based on the approximate incidence angles to obtain an acceptable MV of intensity. Here we should note that longer distances measured by lower resolution may fail in any algorithm because of the extremely limited

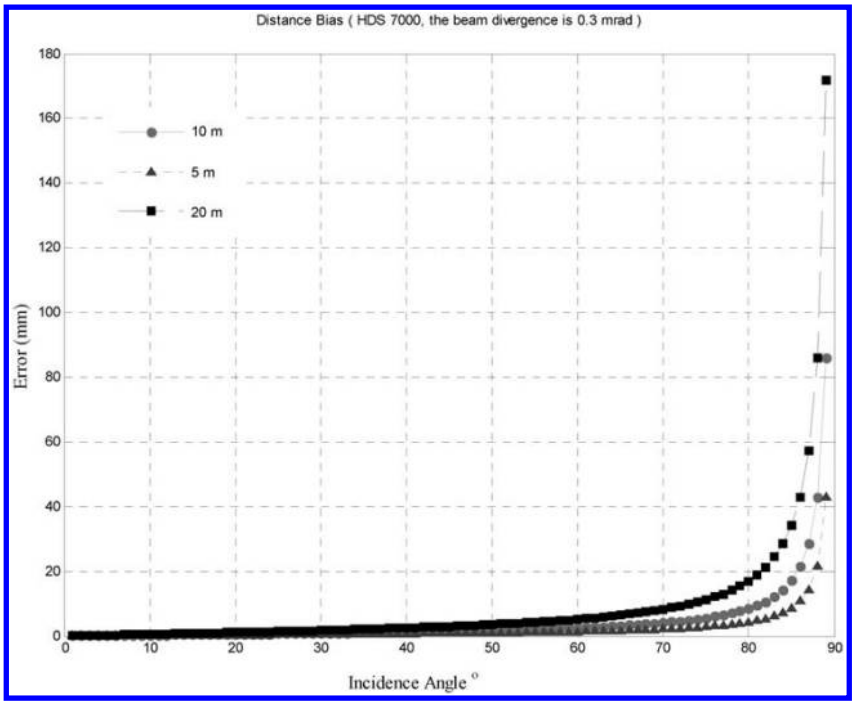

7 Theoretical error influence of incidence angles

sampling. The last histogram in the first row in Fig. 8 also shows this problem and has to be compared with the histogram in the bottom row of the same column where the MV of intensity can be clearly assessed because of increased resolution.

Application examples

Experimental field and instruments

In this section, plane fitting and target centre identification experiments are shown. The tests were performed in the geodetic laboratory at the Technical University of Munich (TUM), and the results were obtained using the TUM's Leica HDS7000 TLS and its standard black and white targets, together with its accompanying software, Cyclone. The range accuracy of HDS7000 from the specification is 1 mm in linearity error and 125 μrad in angular accuracy, both in horizontal and vertical directions. Three levels of resolution are tested: middle, high and super-high levels that contain 5000, 10 000 and 20 000 points in a 360° scan respectively. In the tests for plane fitting, the TUM's Leica Laser Tracker AT901 is

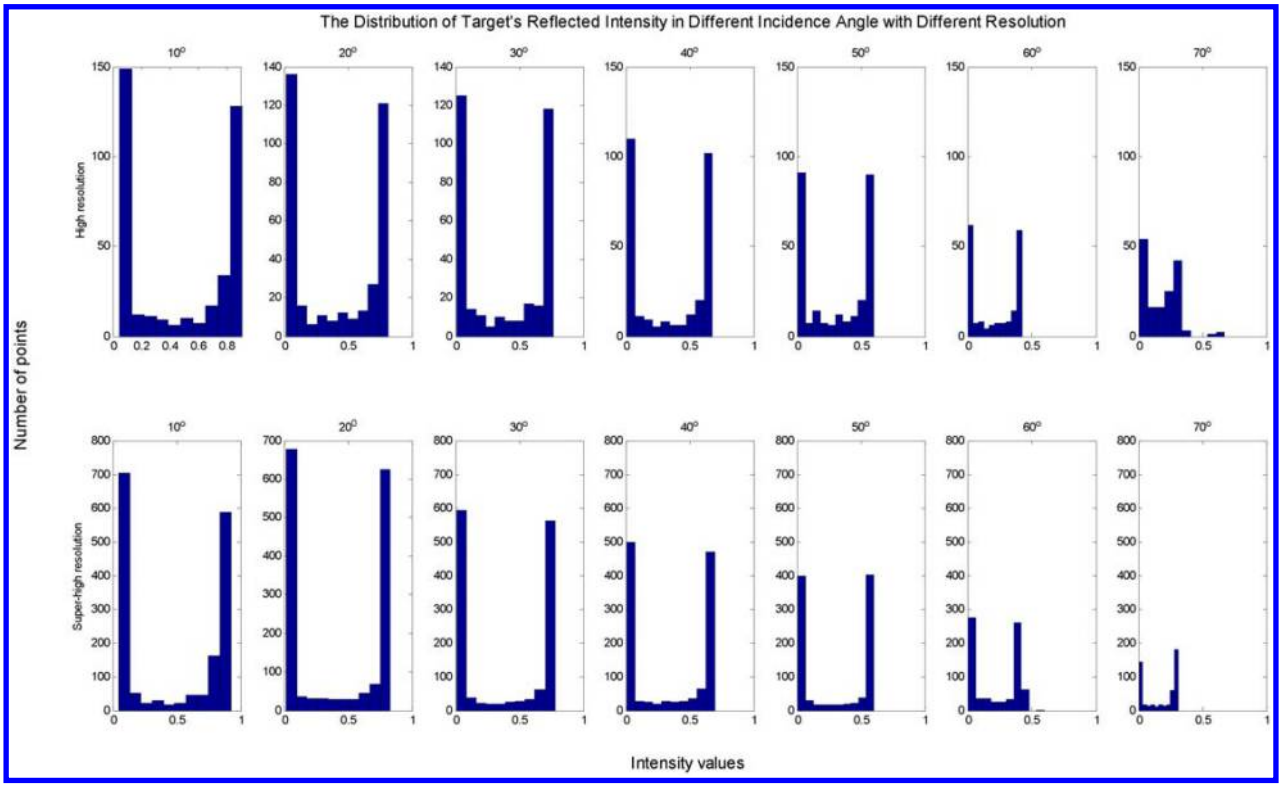

8 Distribution of target's reflected intensity for different incidence angles

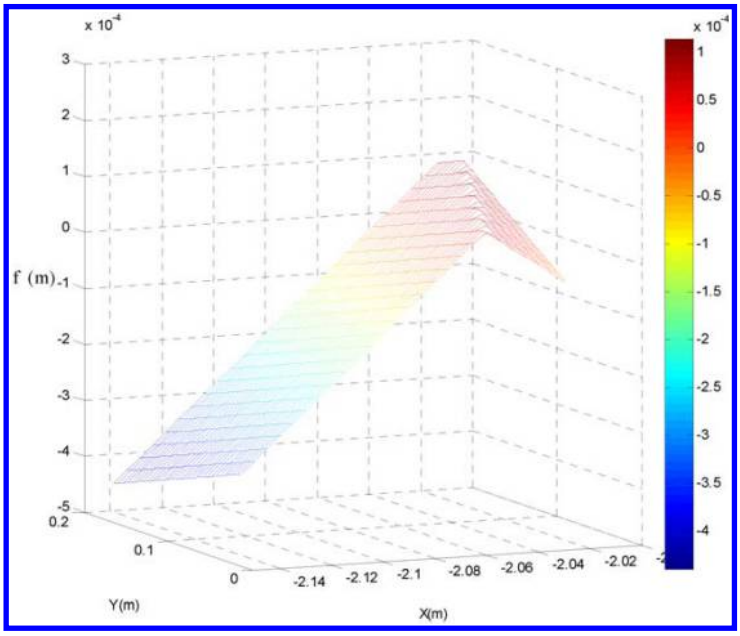

9 Difference in plane fitting by LS and proposed methods

employed to obtain reference planes and to assess the results by different methods. The coordinate component accuracy of the Laser Tracker is 0·01 mm, which is much higher than in the HDS7000. Four control points have been applied to set up the network. As the accuracy of the Laser Tracker is much higher than the HDS7000, the errors in the data of the Laser Tracker can be neglected, and the propagation errors from coordinate transformation can be seen as observation errors from the HDS7000. In the tests of target centre identification, 15 targets are distributed within a range of 21 m on the calibration track line. The purpose of the experiments is to test the applicability of the proposed algorithm in the target identification and to compare the performance of the presented method with the accompanying software. More specifically, the results produced by the accompanying software with super-high resolution are accepted as the 'true' value $\bar{x}$ in the experiments. For the other results, we compute four residuals for each point: three coordinate components' residuals and one point residual, calculated as

$$V_{p_i} = \left(v_{x_i}^2 + v_{y_i}^2 + v_{z_i}^2\right)^{1/2} \tag{20}$$

then, directly compute the corresponding RMSE using the following formula

$$RMSE = \left[\frac{(\hat{x}-\bar{x})^{\mathrm{T}}(\hat{x}-\bar{x})}{m}\right]^{1/2} \tag{21}$$

where in equation (20) V_{p_i} is the ith point residual and v_{x_i}, v_{y_i} and v_{z_i} are corresponding coordinate component residuals. In equation (21), $\hat{x}$ denotes the estimated target centre and m is the number of points.

Experiment 1: plane fitting

Table 1 shows the results of parameter estimation of a target plane fitting by different instruments and methods. The results calculated by least squares (LS) and the proposed methods with TLS data are both compared with those calculated by the Laser Tracker data. In this case, the proposed method produces better results than the LS by 85, 66 and 84% corresponding to the unknown parameters a, b, and c respectively. We keep the plane in target size, specifically, the ranges of the x- and y-axes are respectively between the minimum to maximum with a step of 5 mm. Three fitting planes can be established with calculated parameters respectively

$$\mathbf{z} = a_1\mathbf{x} + b_1\mathbf{y} + c_1 \text{ Laser Tracker : Plane } \mathbf{Z}_1 \tag{22a}$$

$$\mathbf{z} = a_2\mathbf{x} + b_2\mathbf{y} + c_2 \text{ Scanner-LS : Plane } \mathbf{Z}_2 \tag{22b}$$

$$\mathbf{z} = a_3\mathbf{x} + b_3\mathbf{y} + c_3 \text{ Scanner-proposed : Plane } \mathbf{Z}_3 \tag{22c}$$

As the ranges in the x- and y-axes are approximately the same, we can directly compare the z-component to express the mutual positional relationship among the three planes

$$f = |\mathbf{Z}_1 - \mathbf{Z}_3| - |\mathbf{Z}_1 - \mathbf{Z}_2| \tag{23}$$

where, if $f<0$ means plane $\mathbf{Z}_3$ is closer to plane $\mathbf{Z_1}$ than plane $\mathbf{Z}_2$. Figure 9 shows the f values of the 1st target. From those Tables and the figure, we can see that:

(i) the proposed method performs better than the classical method in plane fitting, in other words the proposed method is more robust and can obtain more reliable estimated parameters
(ii) the fitting planes calculated by the presented method are mostly closer to the reference planes

Table 1 Estimated plane parameters using LS and proposed methods

Instrument–method	*a*	*b*	*c*
Laser Tracker	−0·679268571318044	−0·004125952154429	−4·854950961251349
Scanner-LS	−0·682993830461783	−0·003167355073060	−4·862618464369007
Scanner-proposed	−0·678711303485737	−0·003795317961655	−4·853759263364638
Improvement/%	85	66	84

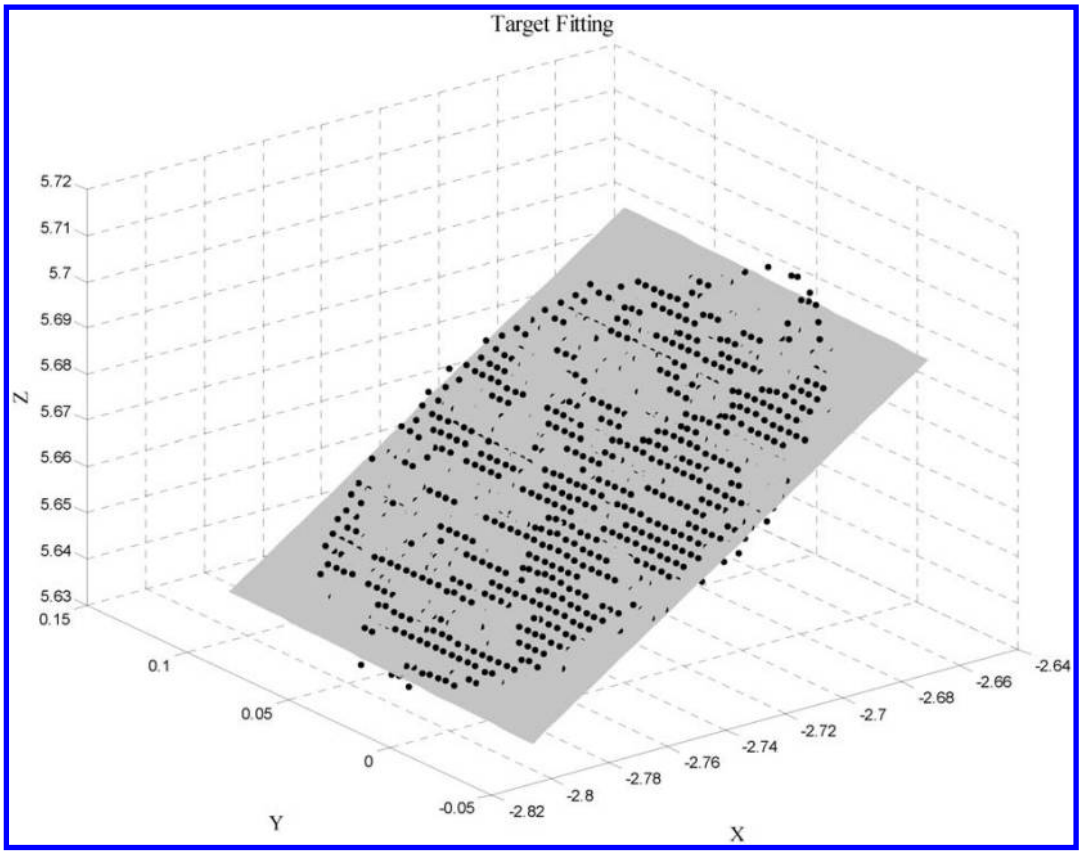

10 Resulting plane by proposed method

than that delivered by the LS, especially the middle part of the planes which is always closer to the reference planes by the proposed method, which will directly influence the accuracy of the following target centre identification

(iii) because the distance is limited to 3 m and scans with super-high resolution do not show the numerical difference of the results between the proposed method and LS clearly in this case with a resolution of 0·1 mm, that difference will become obvious if the distance increases or the resolution decreases

(iv) there contain some parts with positive values, e.g. the red part in Fig. 9, in the edge of target which are caused by the ductility of the plane and the intersection of planes, but have little influence in the centre identification. Figure 10 displays one of the resulting planes by the proposed method.

Experiment 2: centre identification

We offer the Cyclone results and our method results in detail in Tables 4 and 5 in the Appendix respectively, in order to allow readers to repeat the experiments. With the super-high and high resolutions, all targets can be

Table 2 Biases of coordinate components and position respective with high and middle resolutions by Cyclone

Bias/mm

	High model				Middle model				
	Coordinate component			Point	Coordinate component			Point	Dis/m
No.	Δx	Δy	Δz	ΔP	Δx	Δy	Δz	ΔP	D
1	0	0	0	0·0	−1	0	0	1·0	1·8531
2	0	1	0	1·0	0	0	0	0·0	3·3967
3	0	0	0	0·0	0	0	−1	1·0	4·8625
4	0	0	0	0·0	0	0	−1	1·0	6·2961
5	0	0	0	0·0	0	0	0	0·0	7·8011
6	0	1	1	1·4	0	1	−3	3·2	9·3189
7	0	1	0	1·0	−2	−1	1	2·4	10·6149
8	1	0	0	1·0	−2	−1	−2	3·0	11·9215
9	0	0	−1	1·0	2	0	−4	4·5	13·2987
10	0	0	−1	1·0	4	2	−3	5·4	14·6879
11	1	0	0	1·0	1	−1	−7	7·1	16·3394
12	1	1	−1	1·7	3	1	−3	4·4	17·7700
13	−1	−1	2	2·4	…	…	…	…	19·0568
14	−1	−1	0	1·4	…	…	…	…	20·4610
15	1	0	−2	2·2	…	…	…	…	21·9748
RMSE	0·63	0·63	0·89	1·26	1·80	0·87	2·74	3·50	…

identified in our experiments, however, when the scanner uses the middle resolution, the targets in position nos. 13–15 cannot be accurately found or even found at all. Table 2 presents the bias of each coordinate component and the corresponding position bias in detail, between the 'true' values and the results by Cyclone with lower resolutions. According to Table 2, we can see that:

(i) the results by Cyclone with high resolution show just a little difference from the 'true' values, and the biases are 1 mm more or less. The RMSEs of each coordinate component are less than 1 mm and those of the position are slightly larger than 1 mm
(ii) the errors in the results by Cyclone with a middle resolution show an upward trend as the distance increases.

The points from no. 1 to no. 5 contain errors at the same level with that obtained by the high model, while after point no. 5 the errors noticeably increase. The average positional error for points from no. 6 to no. 9 is 3·28 mm and from nos. 10–12 is 5·35 mm. The RMSE of the position is 3·50 mm, which means the accuracy of the position decreases by about 178% compared with the high resolution value, which amounts to 1·26 mm.

Like the results by Cyclone, the targets from nos. 13–15 cannot be accurately found due to of the limited number of points in the proposed method. Table 3 gives a comparison between the results of our proposed method with different resolutions and the 'true' values. Based on Table 3, we can make the following observations. First, with super-high resolution, the proposed method can obtain almost the same results as the 'true' values. The RMSE of each coordinate component is 0·5 mm more or less, and the RMSE of the position is lower than 1 mm. In engineering measurement or even in precision engineering measurement, the results calculated by our proposed method can be accepted with the same accuracy level as 'true' values. Second, With high resolution, the proposed method can also obtain reliable results, the RMSE of each coordinate component is also lower than 1 mm, and the same index for the position is slightly larger than 1 mm. Moreover, these results perform almost at the same level as those obtained by Cyclone with the same resolution. Third, With a middle resolution, the proposed method can obtain reliable results in the first five points; from the no. 6 point, the positional error becomes larger than 2 mm. The RMSE of position is 2·76 mm, which means the accuracy increases by 21·14%, compared with that index obtained by Cyclone with the same resolution.

Figure 11 displays four target centres of target no. 8 captured by four methods in the *z*-*x* perspective. The black and grey squares express the centre obtained by Cyclone and our proposed method respectively. Obviously, these two squares are very close, almost overlapping. The black triangle represents the centre obtained by the radiometric centre of all returns (Lichti *et al.*, 2000), and the grey triangle represents the centre captured by MVC. Clearly, these two centres deviate from the 'true' value of centre.

Conclusions

In this work, we proposed an alternative method for target identification in TLS measurement. In the proposed method, the weighted total least squares method is

Table 3 Biases of coordinate components and position respective with super high, high and middle resolutions by proposed method

Super high model

	Bias/mm				
	Coordinate component			Point	Dis/m
No.	Δx	Δy	Δz	ΔP	D
1	0	0	0	0·0	1·8531
2	0	0	0	0·0	3·3967
3	0	0	0	0·0	4·8625
4	0	0	−1	1·0	6·2961
5	0	0	0	0·0	7·8011
6	0	1	0	1·0	9·3189
7	0	1	0	1·0	10·6149
8	0	0	0	0·0	11·9215
9	0	0	0	0·0	13·2987
10	0	0	0	0·0	14·6879
11	1	0	0	1·0	16·3394
12	0	0	−1	1·0	17·7700
13	0	1	1	1·4	19·0568
14	0	1	−1	1·4	20·4610
15	−1	0	0	1·0	21·9748
RMSE	0·37	0·51	0·52	0·81	…

High model

	Bias/mm				
	Coordinate component			Point	Dis/m
No.	Δx	Δy	Δz	ΔP	D
1	0	0	0	0·0	1·8531
2	0	0	0	0·0	3·3967
3	0	0	−1	1·0	4·8625
4	0	0	0	0·0	6·2961
5	0	0	0	0·0	7·8011
6	0	0	−1	1·0	9·3189
7	0	1	0	1·0	10·6149
8	0	0	1	1·0	11·9215
9	0	0	0	0·0	13·2987
10	−1	1	−1	1·7	14·6879
11	1	1	1	1·7	16·3394
12	0	1	1	1·4	17·7700
13	0	0	1	1·0	19·0568
14	0	1	−1	1·4	20·4610
15	−1	1	1	1·7	21·9748
RMSE	0·45	0·63	0·77	1·09	…

Middle model

	Bias/mm				
	Coordinate component			Point	Dis/m
No.	Δx	Δy	Δz	ΔP	D
1	0	0	0	0·0	1·8531
2	0	1	0	1·0	3·3967
3	0	0	0	0·0	4·8625
4	0	0	0	0·0	6·2961
5	−1	0	0	1·0	7·8011
6	−1	0	−2	2·2	9·3189
7	1	1	2	2·4	10·6149
8	−1	0	2	2·2	11·9215
9	0	0	−2	2·0	13·2987
10	0	1	3	3·2	14·6879
11	−4	−1	−2	4·6	16·3394
12	−5	−2	3	6·2	17·7700
RMSE	1·94	0·82	1·78	2·76	…

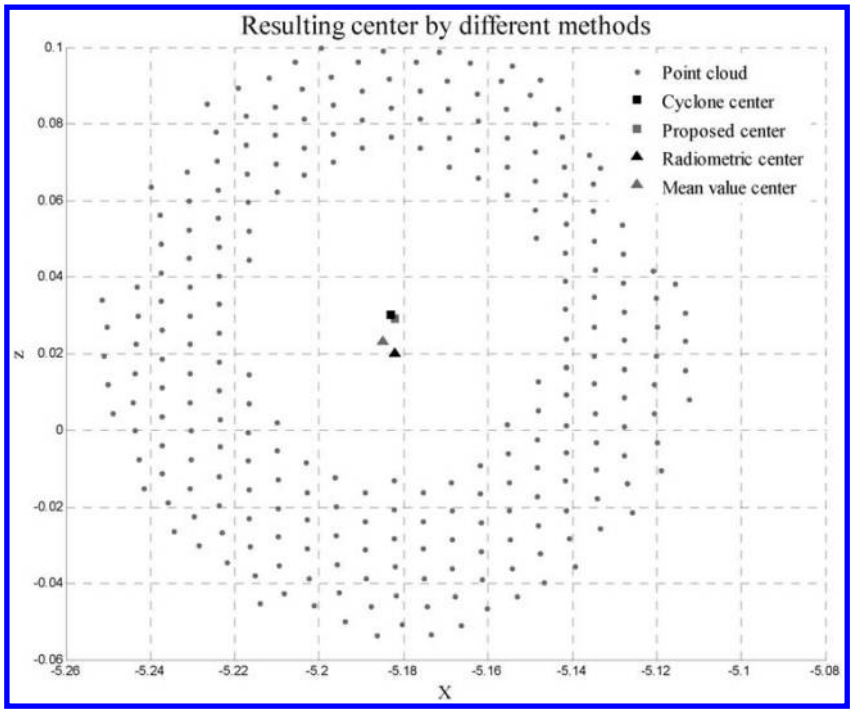

11 Four estimated target centres by different methods

employed to obtain an optimum fitting plane. The planarity condition of the plane is introduced in the plane fitting algorithm to control the accuracy of the resulting plane. After the first step, the characteristics of reflected intensity between different colours are applied to select appropriate points and then project them to the 2D coordinate system. Finally, through a robust iterative calculation, the target centre can be successfully obtained.

The analysis of the experimental results demonstrates the applicability of the proposed method in target identification. From the case study results, we draw the following conclusions.

1. The accuracy of results by arbitrary accompanying software (in our case, Cyclone) is reduced due to lower resolution or increased distance. Therefore, using accompanying software to obtain target centre cannot obtain the best results in all situations. Considering the accuracy requirement and time consumption in each engineering project, choosing the optimum resolution model is very important.

2. The method proposed here can obtain approximately the same accuracy level as that returned by the accompanying software within the range of the tests but just uses common information to complete the target identification process. This gives users increased scope to improve target identification.

3. Furthermore, this method is objectively equal for all manufacturers' instruments; thus, users can objectively compare different instruments' behaviour with respect to target identification. It should be repeated that the quality of target identification directly influences registration quality and has high importance.

Appendix

Table 4 Target centres obtained by Cyclone with different resolutions

Cyclone/m

	Super high (true)				High				Middle			
No.	*x*	*y*	*z*	Point no.	*x*	*y*	*z*	Point no.	*x*	*y*	*z*	Point no.
1	−0·806	1·670	0·028	52046	−0·806	1·670	0·028	13325	−0·805	1·670	0·028	3303
2	−1·476	3·060	0·028	16097	−1·476	3·059	0·028	3944	−1·476	3·060	0·028	963
3	−2·114	4·378	0·028	7847	−2·114	4·378	0·028	2063	−2·114	4·378	0·029	466
4	−2·737	5·669	0·028	4468	−2·737	5·669	0·028	1200	−2·737	5·669	0·029	323
5	−3·392	7·024	0·029	3134	−3·392	7·024	0·029	771	−3·392	7·024	0·029	187
6	−4·052	8·391	0·029	2150	−4·052	8·390	0·030	571	−4·052	8·390	0·032	138
7	−4·615	9·559	0·030	1707	−4·615	9·558	0·030	448	−4·613	9·560	0·029	111
8	−5·182	10·736	0·030	1323	−5·183	10·736	0·030	336	−5·180	10·737	0·032	91
9	−5·782	11·976	0·029	1058	−5·782	11·976	0·030	286	−5·784	11·974	0·033	73
10	−6·386	13·227	0·029	896	−6·386	13·227	0·030	256	−6·390	13·225	0·032	60
11	−7·104	14·714	0·031	729	−7·105	14·714	0·031	184	−7·105	14·715	0·038	49
12	−7·728	16·003	0·031	588	−7·729	16·002	0·032	162	−7·731	16·002	0·028	34
13	−8·283	17·154	0·033	548	−8·282	17·155	0·031	140	…	…	…	…
14	−8·897	18·426	0·030	432	−8·896	18·427	0·030	116	…	…	…	…
15	−9·555	19·790	0·032	372	−9·556	19·790	0·034	103	…	…	…	…

Table 5 Target centres obtained by proposed method with different resolutions

Proposed method/m

	Super high				High				Middle			
No.	*x*	*y*	*z*	Point no.	*x*	*y*	*z*	Point no.	*x*	*y*	*z*	Point no.
1	−0·806	1·670	0·028	52046	−0·806	1·670	0·028	13325	−0·806	1·670	0·028	3303
2	−1·476	3·060	0·028	16097	−1·476	3·060	0·028	3944	−1·476	3·059	0·028	963
3	−2·114	4·378	0·028	7847	−2·114	4·378	0·029	2063	−2·114	4·378	0·028	466
4	−2·737	5·669	0·029	4468	−2·737	5·669	0·028	1200	−2·737	5·669	0·028	323
5	−3·392	7·024	0·029	3134	−3·392	7·024	0·029	771	−3·391	7·024	0·029	187
6	−4·052	8·390	0·029	2150	−4·052	8·391	0·030	571	−4·051	8·391	0·031	138
7	−4·615	9·558	0·030	1707	−4·615	9·558	0·030	448	−4·616	9·558	0·028	111
8	−5·182	10·736	0·030	1323	−5·182	10·735	0·029	336	−5·181	10·737	0·028	91
9	−5·782	11·976	0·029	1058	−5·782	11·976	0·029	286	−5·782	11·976	0·031	73
10	−6·386	13·227	0·029	896	−6·385	13·226	0·030	256	−6·386	13·226	0·026	60
11	−7·105	14·714	0·031	729	−7·105	14·713	0·030	184	−7·100	14·715	0·033	49
12	−7·728	16·003	0·032	588	−7·728	16·002	0·030	162	−7·723	16·005	0·028	34
13	−8·283	17·153	0·032	548	−8·284	17·154	0·032	140	…	…	…	…
14	−8·897	18·425	0·031	432	−8·897	18·425	0·031	116	…	…	…	…
15	−9·554	19·790	0·032	372	−9·554	19·789	0·031	103	…	…	…	…

References

Ebeling, A., Chow, J. and Teskey, W. F., 2011. Deformation analysis of terrestrial monitoring observations on Turtle Mountain, Alberta. *Journal of Applied Geodesy*, 5(1), 47–58.

Gordon, S. J., Lichti, D. D. and Stewart, M., 2001. Application of a high-resolution, ground-based laser scanner for deformation measurements. In: *Proc. 10th FIG International Symposium on Deformation Measurements*, Orange, CA, USA, 19–22 March.

Gordon, S. J., 2005. *Structural deformation measurement using terrestrial laser scanners*. Ph. D. Curtin University of Technology, Australia.

Gordon, S. J. and Lichti, D., 2007. Modeling terrestrial laser scanner data for precise structural deformation measurement. *J. Surv. Eng.*, 133(2), 72–80.

Granthamn, J. W. *et al.*, 1997. Laser radar in adverse weather. In: *SPIE Proceedings*, Vol. 3065, 84–93.

Kaasalainen, S. *et al.*, 2005. Study of surface brightness from backscattered Laser intensity calibration of Laser data. *IEEE Geosci. Remote Sens. Lett.*, 2(3), 255–259.

Kersten, T. H. *et al.*, 2004. Terrestrial lasers canning system MENSI GS 100/GS200 – accuracy tests, experiences and projects at the Hamburg University of applied Sciences. In: *Proc. Panoramic Photogrammetry Workshop 2004*, TU Dresden, University of Stuttgart, and ISPRS WG V/1, February, 19–22.

Konstantionv, M., Mehrmann, V. and Petkov, P., 2000. On properties of Sylvester and Lyapunov operators. *Linear Algebra Appl.*, 312(1–3), 35–71.

Kremen, T., Koska, B. and Pospsil, J., 2006. Verification of laser scanning systems quality. In: *Proc. in the XXIII FIG Congress*, Shaping the Change, Munich, Germany.

Lichti, D. D. *et al.*, 2000. Benchmark tests on a three-dimensional laser scanning system. *Geomat Res Australas*, 72, 1–24.

Lichti, D. D. and Harvey, B. R. 2002. An investigation into the effects of reflecting surface material properties on TLS measurements. *Geomat Res Australas*, 76, 1–6.

Lichti, D. D. and Gordon, S. J., 2004. Error propagation in directly georeferenced terrestrial laser scanner point cloud for cultural heritage recording. In: *Proc. of FIG Working Week*, Athens, Greece, May 22–27.

Lichti, D. D., 2007. Error modelling, calibration and analysis of an AM-CW terrestrial laser scanner. *ISPRS Journal of Photogrammetry and Remote Sensing*, 61(5), 307–324.

Schaffrin, B. and Wieser, A. 2008. On weighted total least-squares adjustment for linear regression. *J. Geodesy*, 82(7), 415–421.

Soudarissanane, S. *et al.*, 2009. Incidence angle influence on the quality of terrestrial laser scanning points. *Laser Scanning*, 35(3/W8), 183–88.

Soudarissanane, S. *et al.*, 2011. Scanning geometry: influencing factor on the quality of terrestrial laser scanning points. *ISPRS Journal of Photogrammetry and Remote Sensing*, 66(4), 389–99.

Staiger, R., 2005. The geometrical quality of laser scanner (TLS). In: *Proc. of FIG Working Week 2005 and GSDI-8*, Cairo, Egypt, 16–21 April.

Thiel, K.-H. and Wehr, A., 2004. Performance capabilities of laser scanners – an overview and measurement principle analysis. In: *Proceedings of the ISPRS working group VIII/2 'Laser scanner for Forest and landscape assessment'*, Freiburg, Germany, 3–6 October.

Randall, T., 2011. Construction engineering requirements for integrating laser scanning technology and building information modeling. *Journal of Construction Engineering and Management*, 137(10), 797–805.

Reshetyuk, Y., 2006. Calibration of terrestrial laser scanner Callidus1·1, Leica HDS3000 and Leica HDS2500. *Survey Review*, 38(302), 703–13.

Reshetyuk, Y., 2010. A unified approach to self-calibration of terrestrial laser scanners. *ISPRS Journal of Photogrammetry and Remote Sensing*, 65(1), 445–56.

Valanis, A. and Tsakiri, M., 2004. Automatic target identification for laser scanners. In: *Proc. of the XXth ISPRS Congress*, Istanbul, Turkey, 12–23 July.

Zhou W. J., 1989. Classical theory of error and Robust estimation. *Acta Geodaeticaet Cartographica Sinica*, 18(2), 115–20.